

Air Force Institute of Technology

AFIT Scholar

Faculty Publications

3-2022

Computational Based Investigation of Lattice Cell Optimization under Uniaxial Compression Load

Derek G. Spear

Jeremiah S. Lane

Anthony N. Palazotto

Air Force Institute of Technology

Ryan A. Kemnitz

Air Force Institute of Technology

Follow this and additional works at: <https://scholar.afit.edu/facpub>

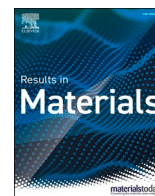


Part of the [Engineering Science and Materials Commons](#), and the [Manufacturing Commons](#)

Recommended Citation

Spear, D. G., Lane, J. S., Palazotto, A. N., & Kemnitz, R. A. (2022). Computational based investigation of lattice cell optimization under uniaxial compression load. *Results in Materials*, 13, 100242. <https://doi.org/10.1016/j.rinma.2021.100242>

This Article is brought to you for free and open access by AFIT Scholar. It has been accepted for inclusion in Faculty Publications by an authorized administrator of AFIT Scholar. For more information, please contact richard.mansfield@afit.edu.



Computational based investigation of lattice cell optimization under uniaxial compression load[☆]

Derek G. Spear^{a,*}, Jeremiah S. Lane^b, Anthony N. Palazotto^a, Ryan A. Kemnitz^a

^a Air Force Institute of Technology, Department of Aeronautics and Astronautics, 2950 Hobson Way, Wright-Patterson AFB, OH, 45 433, USA

^b Air Force Institute of Technology, Department of Mathematics, 2950 Hobson Way, Wright-Patterson AFB, OH, 45 433, USA

ARTICLE INFO

Keywords:

Topology optimization
Additive manufacturing
Triply periodic minimal surfaces (TPMS)
Lattices

ABSTRACT

Structural optimization is a methodology used to generate novel structures within a design space by finding a maximum or minimum point within a set of constraints. Topology optimization, as a subset of structural optimization, is often used as a means for light-weighting a structure while maintaining mechanical performance. This article presents the mathematical basis for topology optimization, focused primarily on the Bi-directional Evolutionary Structural Optimization (BESO) and Solid Isotropic Material with Penalization (SIMP) methodologies, then applying the SIMP methodology to a case study of additively manufactured lattice cells. Three lattice designs were used: the Diamond, I-WP, and Primitive cells. These designs are all based on Triply Periodic Minimal Surfaces (TPMS). Individual lattice cells were subjected to a uniaxial compression load, then optimized for these load conditions. The optimized cells were then compared to the base cell designs, noting changes in the stress field response, and the maximum and minimum stress values. Overall, topology optimization proved its utility under this loading condition, with each cell seeing a net gain in performance when considering the volume reduction. The I-WP lattice saw a significant stress reduction in conjunction with the mass and volume reduction, marking a notable increase in cell performance.

1. Introduction

Structural optimization is a mathematical approach of fundamental interest to the engineering field due to its potential for future growth and development. At its core, optimization is concerned with maximizing or minimizing certain properties given specific loading conditions and constraints on the structure. The subject of structural optimization is broken into three separate but related sub-domains: size optimization, shape optimization, and topology optimization. In engineering applications, these three sub-domains are often treated separately. The size and shape of a structure are typically determined by utility and requirements, having a minimal design space available to consider. Thus, topology optimization is of utmost interest when attempting to construct the most effective design of structures.

While the shape and size of a given structural design are well understood, the consideration of topology to the design process is much more esoteric. Geometrically, topology is concerned with the arrangement of the material itself within the given structural shape and size. As

the goal is generally to maximize a specific structural or mechanical quality while minimizing the amount of material required, a firm understanding of the applicable principles of topology optimization is necessary.

The first step in preparing a structure for a topology optimization analysis is to understand the design space. That is, the nature of design decisions made throughout the topology optimization must be formalized. This aim is achieved by performing a finite element analysis (FEA) on the structure. The continuum design space is partitioned into a mesh of discrete elements of finite size within the prescribed shape and size. Then a structural analysis is carried out on the elements. This type of analysis is widely used within the field of mechanics, and thus a variety of tools and software packages exist for FEA, such as Abaqus [1] and Fusion 360 [2]. This formulation naturally allows for design decisions based on the property to be optimized and the constraints placed on the structure. That is, for each finite element within the mesh, the determination is made on whether the material should exist as part of the solution or if the mesh volume should be left a void.

[☆] The views expressed in this article are those of the authors and do not reflect the official policy or position of the United States Air Force, Department of Defense, or the US Government.

* Corresponding author.

E-mail address: derek.spear@us.af.mil (D.G. Spear).

<https://doi.org/10.1016/j.rinma.2021.100242>

Received 1 October 2021; Received in revised form 14 November 2021; Accepted 27 November 2021

Available online 1 December 2021

2590-048X/Published by Elsevier B.V. This is an open access article under the CC BY license (<http://creativecommons.org/licenses/by/4.0/>).

The optimization problem can be formulated with the finite element method because it allows the incorporation of design decisions for a structure's topology. Canonically, any optimization problem can be expressed through well-defined design variables, an objective function, and constraints to the size and shape of the structure. The generalized optimization problem is depicted below, where $f(\mathbf{x})$ is the objective function to be minimized, \mathbf{x} is the vector of design variables, and \mathbf{C}_j is the j th constraint to be satisfied by the design variables.

$$\begin{aligned} & \text{Minimize } f(\mathbf{z}) \\ & \text{Subject to :} \\ & \quad \mathbf{C}_j \\ & \quad \mathbf{z}_j = 0 \text{ or } 1 \end{aligned}$$

For a structure subject to extreme loading or extreme boundary conditions, it is of particular interest to explore the microscale effects of the material by which the structure is composed. Historically, topology optimization has been performed under the assumption of linear elastic structures with negligible microscale effects. For larger homogeneous structures undergoing standard loading, it was an effective assumption that permitted more easily calculable solutions. However, with more strenuous engineering requirements, such as a complex starting design like an open cell lattice, it is necessary to consider the microstructure of the material composing the structure. At a fundamental, physical level, every material can be characterized by the structural formation of its atoms. Metals are characterized by the formation of periodic crystal structures composed of their respective atoms. These structures then form the grain microstructure of the metal. The governing behavior of this phenomenon is well understood through materials modeling in physics. As the size of the elastic structure approaches the scale of its constitutive microstructure, the behavior of the microstructure becomes more significant.

The following sections will introduce the mathematical details of the optimization problem and then explore the relationship between the micro and macro scales, discussing potential methods for bridging the gap between them. Two widely used optimization methodologies will be presented in greater detail: Bi-directional Evolutionary Structural Optimization (BESO) and Solid Isotropic Material with Penalization (SIMP). After discussing these methods, an optimization study involving three Triply Periodic Minimal Surface (TPMS) lattice cells will be presented.

The decision to optimize lattice cells is based on the growing interest in the mechanical properties of additively manufactured metal lattice structures to meet specific engineering needs. Early work in this area was performed by Körner through experimentation of additive fabrication methods and materials to characterize the quality of the manufacturing process for both method and material [3]. Al-Ketan et al. performed a variety of compressive mechanical characterization testing on strut, skeletal, and surface-based lattices additively manufactured out of steel, comparing the mechanical properties between lattice types and cellular designs [4–6]. Recent research has expanded into characterizing the compression mechanical behavior of surface-based lattices fabricated out of Inconel 718 (IN718), with a more focused investigation of the designs' energy absorption characteristics to be used in survivability applications [7–9]. Asadpoure et al. performed some of the early work in the topology optimization of additively manufactured metal lattices, although their work focused on two-dimensional representations of the lattice design [10,11]. Du et al. used topology optimization to improve the shear stiffness of lattice cells employing a two-dimensional energy-based technique focused on the lattice microstructure [12]. Liu et al. further developed this research area by expanding their two-dimensional representations into three-dimensional space [13]. Hanks and Frecker developed a three-dimensional ground structure topology optimization approach to optimize a unit cell for additively manufactured heat sink applications [14]. Additional research has been performed on three-dimensional lattice topology manipulation by evaluating variational designs of TPMS cells through modification of the

trigonometric expressions for each cell design [15]. The present work aims to expand upon this latest research utilizing topology optimization methods on three-dimensional lattice cells to develop new designs for consideration in engineering and design applications.

2. Multiscale model

To formulate the topology optimization problem while accounting for both the macroscale and microscale effects within the structure, the first-order homogenization method, FE_2 , will be considered [16]. This method assumes a distinct separation of the treatment of the two spatial scales, including their periodicity assumptions. The procedure seeks to attain macroscale equilibrium within the structure given an initial loading condition. The structure is assumed to be homogeneous at the macroscale, wherein each discrete finite element maintains unknown structural characteristics to be determined by the constitutive microstructure. Fig. 1 provides a visual representation for the characterization of the structural macroscale and material microscale.

For a given material, the potential relationship as a function of microstructure strain is assumed to be known, where the microstructure stress is the partial derivative of the potential function with respect to strain:

$$\sigma(\epsilon) = \frac{\partial \omega(\epsilon)}{\partial \epsilon} \quad (1)$$

Next, periodic boundary conditions for each structural element within the finite element framework are established. Iteratively, given the initial loading conditions, the microstructure strain at each discrete material point within the discrete structural point is set equal to the structural average strain value, or mean strain, represented by $\bar{\epsilon}$ [18]. Letting \mathbf{X} denote the spatial position of the macroscale element, and letting \mathbf{x} denote the position of the microscale element within the structural element, the following relation is established:

$$\epsilon(\mathbf{X}, \mathbf{x}) = \bar{\epsilon}(\mathbf{X}) \quad (2)$$

Employing this relation, the microstructure stress, $\sigma(\mathbf{X}, \mathbf{x})$, is then calculated using Eqn. (1) [18]. The macroscale stress at each structural element is then found by taking the mean stress, $\bar{\sigma}$, across the material elements through means of volume averaging across the interfacing elements:

$$\sigma(\mathbf{X}) = \bar{\sigma}(\mathbf{X}, \mathbf{x}) \quad (3)$$

This method assumes small displacements within the macrostructure. It proceeds to calculate the tangent stiffness tensor and subsequently update the macroscale displacement using a numerical technique, such as the Newton-Raphson Method, which is used in the FE_2 methodology. The macrostructure is determined to be in a state of equilibrium when the divergence of the Cauchy stress tensor, $\sigma(\mathbf{X})$ is

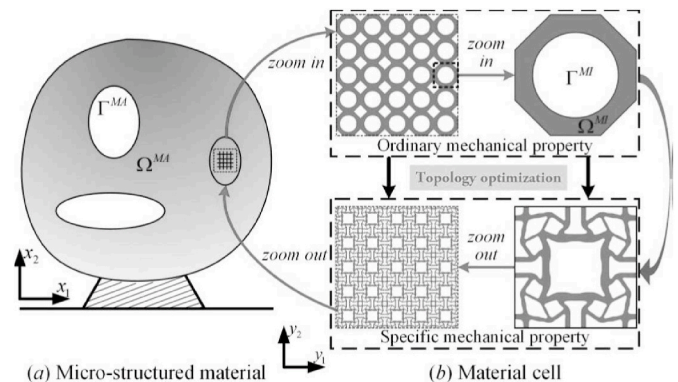


Fig. 1. Relationship between macrostructure and microscale material properties [17].

zero at every structural element,

$$\nabla \cdot \sigma(\mathbf{X}) = \begin{bmatrix} \frac{\partial \sigma_{xx}}{\partial x} & \frac{\partial \sigma_{yx}}{\partial y} & \frac{\partial \sigma_{zx}}{\partial z} \\ \frac{\partial \sigma_{xy}}{\partial x} & \frac{\partial \sigma_{yy}}{\partial y} & \frac{\partial \sigma_{zy}}{\partial z} \\ \frac{\partial \sigma_{xz}}{\partial x} & \frac{\partial \sigma_{yz}}{\partial y} & \frac{\partial \sigma_{zz}}{\partial z} \end{bmatrix} = 0 \quad (4)$$

and the Cauchy stress tensor is equal to the external Cauchy traction vector, \mathbf{t} , along the structural boundary:

$$\mathbf{t} = \sigma \cdot \mathbf{n} \quad (5)$$

In essence, this method establishes an equilibrium between the structural macroscale, characterized by the potential energy of the external forcing, and material microscale effects, described by the potential energy of the internal strain, through the implementation of periodic boundary conditions between the two scales, and iteratively updating the macroscale displacements through non-linear elastic analysis while checking that necessary equilibrium conditions are met. Fig. 2 provides a visual depiction of this iteration process.

As might be expected, the iterative nature of the FE₂ methodology for resolving macroscale and microscale effects within a structure comes with a high computational cost. The solution requires storing microscale data within each macroscale element, which increases computer memory requirements, especially for fine finite element meshes. Furthermore, the computation of the macroscale displacement requires numerical root-finding methods, which may require several iterations depending on the desired accuracy.

3. Topology optimization

The conventional optimization problem requires the maximization or minimization of a specific objective function over a set containing design variables subject to a system of constraints that must be met. Design limitations or requirements typically set these constraints. For linear optimization problems, the solution methods are well established and relatively easy to implement. Such problems are solved using linear programming through the simplex algorithm, which evaluates the objective function while traveling along vertices of the n-dimensional polytope bounded by the permissible region established by the constraints on the n decision variables. This procedure assumes a linear relationship between the objective function, system constraints, and design variables. In addition, the method requires that the design space be continuous. For the non-linearly elastic topology optimization problem described in this paper, neither of these conditions are met.

Therefore, non-linear optimization methods must be used to solve the topology optimization problem at hand. By default, discrete topology optimization algorithms within FEA systems have the disadvantage that the product of the optimization is a non-smooth structural geometry. As many engineering applications require smooth geometric shapes, a smoothing procedure has to be performed. Depending on the optimization geometric constraints, the resulting geometry is usually highly organic in form, requiring a manual process of interpreting and implementing the results into a parameterized model suitable for further computational analysis or production.

In developing the topology optimization model, the first consideration that must be precisely determined is what is to be optimized within the structure. For many structural applications within the aerospace industry, interest often lies in minimizing structural deformation due to an applied loading profile within the prescribed size and weight constraints. This phenomenon is captured through the stiffness of the structure, which can be thought of as the structure's resistance to deformation at a given applied load. Due to its importance in application, the focus of this paper will be on the effective maximization of structural stiffness. An equivalent objective to maximizing stiffness is minimizing the mean compliance, or flexibility, of the structure. Mean compliance is defined as:

$$C = \mathbf{f} \cdot \mathbf{u} \quad (6)$$

where \mathbf{f} is the applied load vector acting on the structure and \mathbf{u} is the elemental displacement at the location of the applied load. This objective function is equivalent to minimizing the strain energy of the structure under static loading cases while neglecting other energy effects such as thermal considerations. As structural elements will be added and removed to pursue an optimal topology, the overall system is constrained by the total volume of possible structural elements. That is, the total sum of structural elements must be less than or equal to the total allowable number of structural elements as defined in the finite element discretization of the structure. Additionally, a load equilibrium constraint must be imposed on the structure. The externally applied force must be in equilibrium with the subsequent internal loads experienced within the structure, which can be expressed through the relation:

$$\mathbf{f} - \sum_{i=1}^N x_i \int_{V_i} \mathbf{B}^T \sigma d\Omega_i = 0 \quad (7)$$

where x_i is the i th design variable representing the binary existence of a structural element, \mathbf{B} is the shape function matrix for the element, σ is the Cauchy stress tensor, and Ω_i is the i th structure elemental volume. The topology optimization problem is obtained by combining the objective function with these constraints:

$$\begin{aligned} &\text{Minimize } C = \mathbf{f} \cdot \mathbf{u} \\ &\text{Such that :} \\ &V_{tot} - \sum_{i=1}^N x_i V_i \geq 0 \\ &\mathbf{f} - \sum_{i=1}^N x_i \int_{V_i} \mathbf{B}^T \sigma d\Omega_i = 0 \\ &\text{Where :} \\ &x_i = 0 \text{ or } 1 \end{aligned}$$

Solving such a non-linear, integer programming problem is highly nontrivial and must rely on numerical methods to obtain a solution.

3.1. Bi-directional Evolutionary Structural Optimization

One of the most prominent methods developed to address non-linear, numerical optimization in the past couple of decades is the BESO method. This method is concerned with establishing an algorithm that converges stably towards the optimal solution by simultaneously adding and removing structural elements and evaluating the resulting impact on the objective function. This requires the introduction of an i th

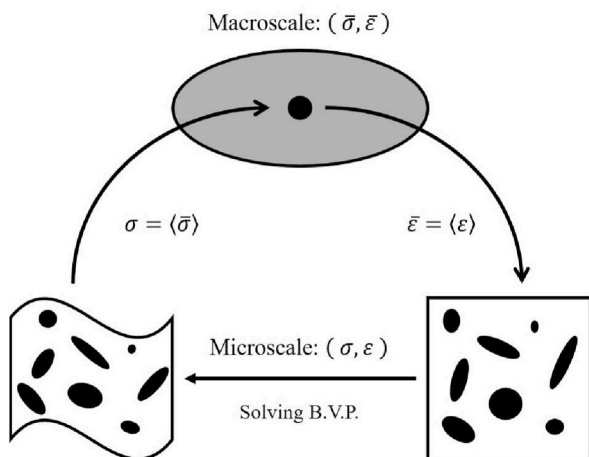


Fig. 2. Iterative solution procedure of the FE₂ methodology.

$$2(\cos mx \cos my + \cos mx \cos mz + \cos my \cos mz) - \cos 2mx \cos 2my \cos 2mz = 0 \tag{13}$$

$$\cos mx + \cos my + \cos mz = 0 \tag{14}$$

In these representations, x , y , and z represent the lattice surface's three-dimensional Cartesian coordinates, and m is the periodicity scaling factor, which sets the number of cells replicated throughout the structural space, which is the ratio of 2π to the cell size. A depiction of each of these three TPMS cell designs is provided in Fig. 3.

The surfaces were then thickened using a surface normal offset of the half-thickness value. These architected surfaces are then used to create a cellular solid of replicated unit cells, as depicted in Fig. 4.

The finite element model was established using a single cell representation based on the experimental uniaxial compression conditions that yielded the mechanical properties for IN718 used within the FEA [8]. As the analysis remained within the linear elastic loading regime for the lattice cells, only the modulus of elasticity and Poisson's ratio of additively manufactured IN718 were used in the analysis. The value for IN718's modulus of elasticity was further refined based on experimental tests of the lattice structures, which were then used in the baseline analysis.

Due to the geometry of the lattice cells, tetrahedral meshes were utilized under the free-structured methodology in Abaqus, based mainly on the surface triangulation technique used in generating the cells. Three-dimensional stress elements of a quadratic geometric order from the Standard Element Library within Abaqus were chosen, specifically the C3D10 M element. This element is a modified 10-noded quadratic tetrahedron that works well in deformation analysis and exhibits minimal shear and volumetric locking. Fig. 5 provides a depiction of the model and mesh for each of the lattice cells.

The simulations were conducted on the individual unit cells by applying a mixed boundary condition scenario to account for both the cell's loading condition and periodicity inside of the cellular solid. When considering the uniaxial compression loading, with the load occurring along the y -axis, boundary conditions must be imposed on the loading and opposing surfaces. In this case, the boundary conditions due to uniaxial loading are:

$$\begin{aligned} u_1|_{y=0} = u_2|_{y=0} = u_3|_{y=0} = 0 \\ u_1|_{y=L} = u_3|_{y=L} = 0 \end{aligned} \tag{15}$$

where L is the unit cell length. Under uniaxial loading, the free, or non-loading, surfaces must be kept flat in order to satisfy the symmetry of the cell, or periodicity, within the overall cellular solid [24,25]. This is done by fixing the non-loading axes and imposing a restraint on the rotational axis that corresponds to the loading axis:

$$\begin{aligned} u_1|_{x,z=0} = u_3|_{x,z=0} = 0 \\ u_1|_{x,z=L} = u_3|_{x,z=L} = 0 \\ w_2|_{x,z=0} = w_2|_{x,z=L} = 0 \end{aligned} \tag{16}$$

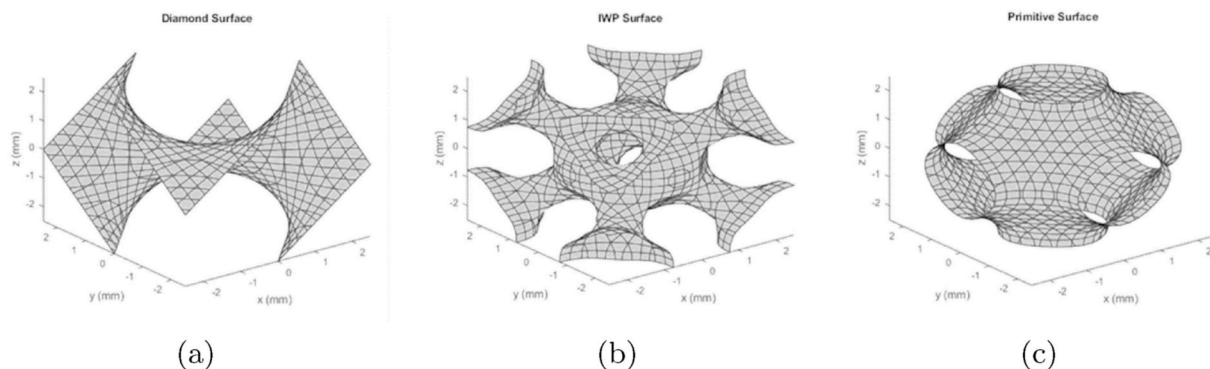


Fig. 3. Single cell TPMS lattice designs: (a) Diamond, (b) I-WP, (c) primitive.

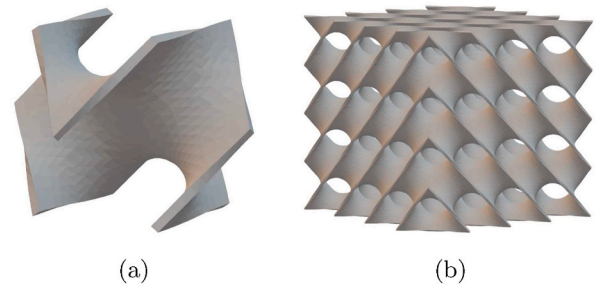


Fig. 4. Diamond TPMS sheet-based lattice: (a) Unit cell, (b) replicated cellular solid.

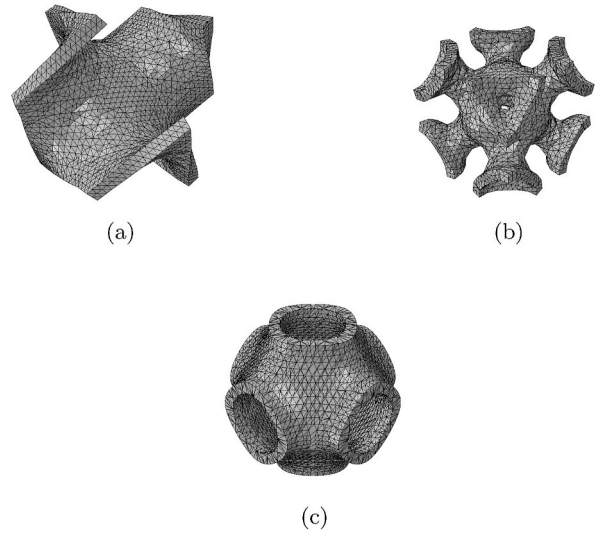


Fig. 5. Single-cell finite element setup and mesh: (a) Diamond lattice, (b) I-WP lattice, (c) primitive lattice.

these mixed boundary conditions provide the uniaxial loading scenario depicted in Fig. 6.

Topology optimization was performed using the same FEA models as previously described incorporating the SIMP methodology for optimization. The chosen objective was to minimize the strain energy present within the unit cell. As the selected loading was considered within the elastic range under static loading, this is equivalent to minimizing the mean compliance of the cell. Within the SIMP options available, the target volume was set to 70% of the original value, a filter radius of 1.3 times the average element edge length was used, the convergence criteria was set at 0.000 1, and element deletion was allowed. Element

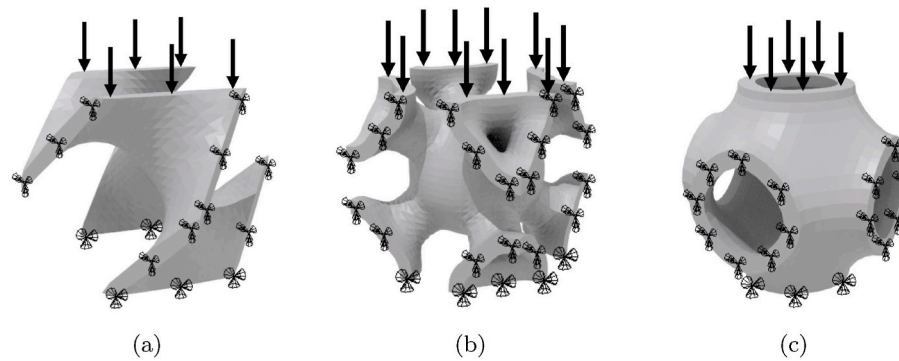


Fig. 6. Mixed boundary conditions for uniaxial compression loading of a unit lattice cell: (a) Diamond lattice, (b) I-WP lattice, (c) primitive lattice.

deletion was based on the sensitivity analysis performed at each loading step; elements with low sensitivity factors, based on low material density factors, lost structural importance and were eliminated from further iterations. Additional constraints were placed upon the free surfaces to prevent element deletion that would cause a break between unit cells within the overall cellular solid.

5. Results and discussion

5.1. Baseline condition

The baseline cells were first analyzed by comparing the uniaxial displacement results of the FEA model to the experimental results [8]. This was done as part of a convergence study of the element size within the model, and to verify the accuracy of the model prior to evaluating the stress field and performing the subsequent optimization. The largest average element size that provided consistent results was selected for simulation to reduce the required computation time. The displacement results are presented in Table 1; the experimental displacement value is the average value for three tests performed on each lattice cell design. As the elastic modulus used in simulation was refined based on the experimental uniaxial compression tests that are being modeled here, the results are very close.

With the model being validated against experimental results, the stress field was analyzed to locate regions of peak stress and note their values. The peak stress was achieved along the edge of the cell surface vertical curve for the Diamond lattice, reaching a maximum value of 656.23 MPa. The minimum stress was found near the adjacent cell connecting edge of the x-z axis, with a value of 0.85 MPa. The I-WP peak stress was located along the inner surface of one of the upper connecting arms, with a peak value of 2,639.07 MPa. Minimum stress for the I-WP cell was 2.81 MPa and situated on the upper exterior surface along the vertical axis. The Primitive peak stress was located along the outer surface of the circular opening that passes between the cells, which was expected to be a stress concentration point based on circular hole theories, and the stress reached a value of 838.54 MPa. The minimum stress value for the Primitive lattice cell was 19.17 MPa and was found along the outer surface between the connecting openings between cells. The stress fields for each of the lattice cell designs can be seen in Fig. 7.

5.2. Optimization

The minimum stress locations within the lattice cell stress field correlate to the minimum load path criticality, which are areas where the objective function is not highly sensitive to the structural element. These regions, in turn, correspond to the regions that will be volume reduced during the optimization process. The uniaxial compression loading used during the optimization process for each cell was carried out over twenty steps, where the load path criticality and element sensitivity were evaluated at each step for volume reduction and stiffness maximization. With the boundary conditions placed on the connecting surface edges, the load path criticality of these edges was increased to prevent element deletion.

The normalized stiffness for the lattice cells was determined at each optimization solution step, then compared to determine the convergence of the solution. The optimization convergence history is provided in Fig. 8. The curves for each cell show an initial decrease in normalized stiffness. This is due to the removal of non-load bearing elements from the initial sensitivity analysis. Once the bulk of non-load bearing elements are removed, the stiffness then increases as the topology optimization reinforces the areas that support the majority of the load. The increase in stiffness is caused by either increasing element volume or the addition of new elements. Each cell type requires a different number of solution steps to achieve a converged state, with the Diamond lattice cell reaching a converged stiffness in 42 steps, while the I-WP needed 55 steps, and the Primitive cell required 73.

The optimization process for the Diamond lattice cell can be seen in Fig. 9, showing the starting load path criticality and reduction to a target volume of 70%. The low-stress regions of the cell along the primary horizontal surface sections were quickly removed within the optimization process. Then the developed void space was further expanded through the incrementation of the process. This resulted in large openings that aligned with the loading direction, while the optimized Diamond lattice cell retained 69.06% of the original cell volume.

The I-WP lattice cell optimization is presented in Fig. 10. In the I-WP lattice cell, there were larger regions of low stress in the base cell loading scenario, which ultimately lead to large openings along the loading direction in the center of the cell, and at each corner through both the upper and lower connection pathways. Further elements were removed from the outer surface of the center region of the cell between the high-stress loading bands running between the upper and lower arms of the cell. The resultant volume of the optimized I-WP lattice cell was 70.02%.

Table 1

Comparison of FEA and experimental uniaxial compression displacement for three lattice cells.

Lattice Cell Design	Compression Load (kN)	Number of FEA Model Elements	FEA Model Compression (mm)	Experimental Compression (mm)	Difference (%)
Diamond	19.57	20,367	0.058 16	0.058 20	-0.06
I-WP	37.84	30,851	0.053 3	0.053 30	0.04
Primitive	19.88	21,389	0.057 13	0.057 10	0.05

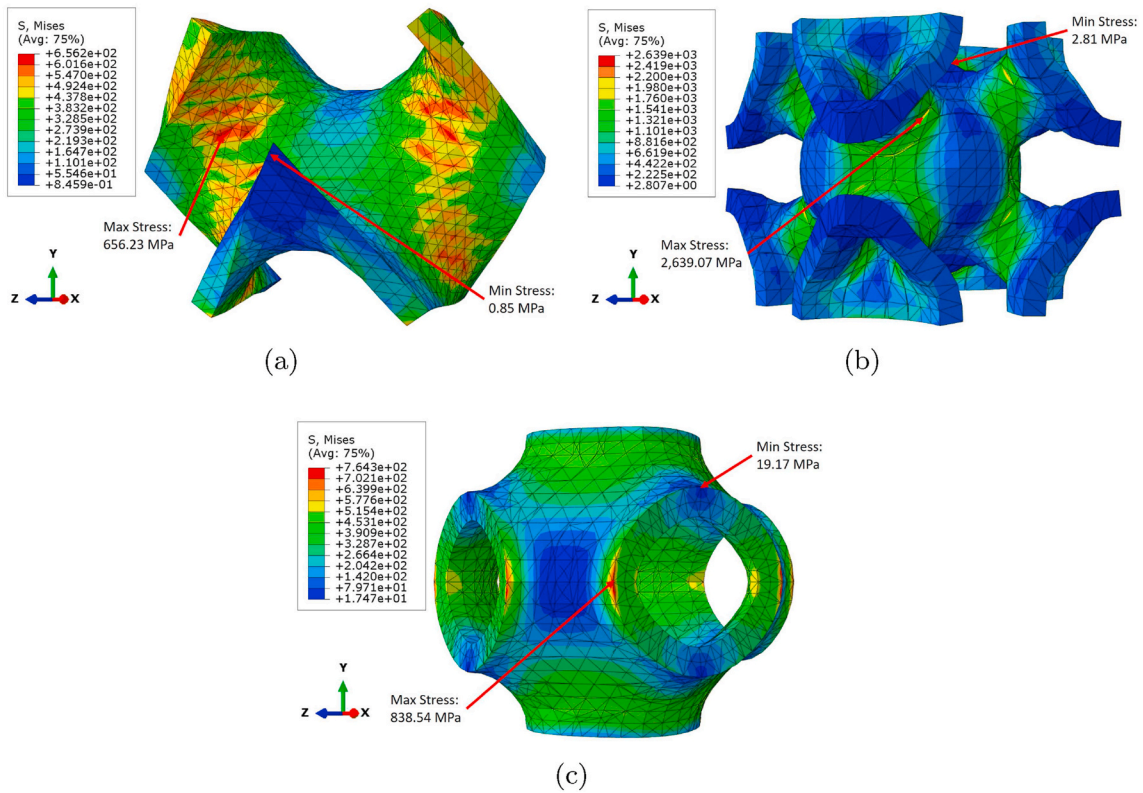


Fig. 7. Stress field under uniaxial compression for unit lattice cell: (a) Diamond lattice, (b) I-WP lattice, (c) primitive lattice.

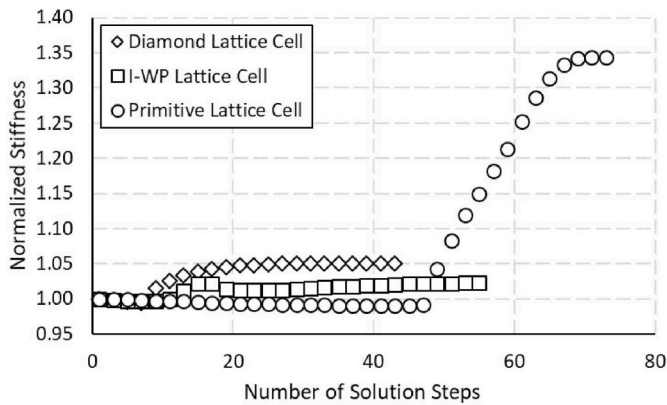


Fig. 8. Convergence of stiffness optimization for TPMS lattice cells.

Finally, the Primitive lattice cell optimization process is shown in Fig. 11. Due to the nature of being a cell of a connected lattice, several low-stress regions of the Primitive cell were not eligible for deletion along the circular connecting openings. This led to a more significant portion of the volume reduction from the connecting arms' upper and lower surfaces. As with the I-WP cell, the remaining volume reduction needed to reach the target 70% volume reduction was taken from the sides of the center region of the cell between the arms. The resultant optimized Primitive lattice cell had void regions develop through the upper and lower surfaces of the connection pathways and a final volume of 75.07%.

5.3. Optimized condition

The optimized cells were then evaluated under the same loading conditions that the base lattice cells were subjected to, maintaining the base material properties. The key to this evaluation was to note changes in the stress field and the peak stress values and locations observed within the cells. A second convergence study was performed for the optimized cells, as the changes in geometry necessitated changes in

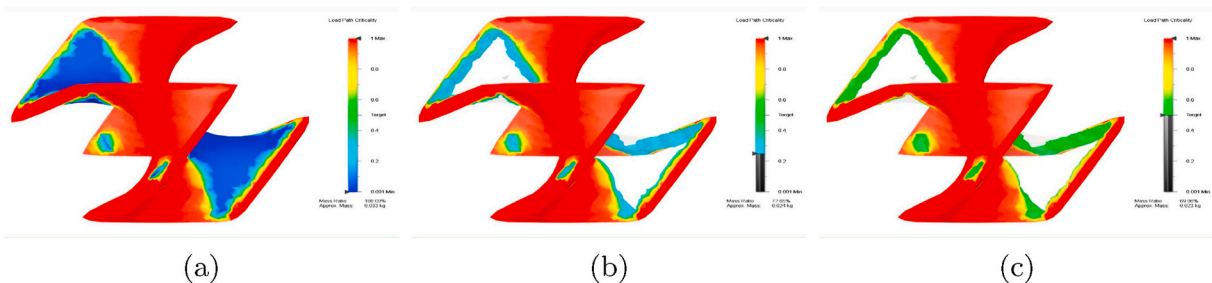


Fig. 9. Diamond lattice cell topology optimization under uniaxial compression loading: (a) 0% volume reduction, (b) 15% volume reduction, (c) 30% volume reduction.

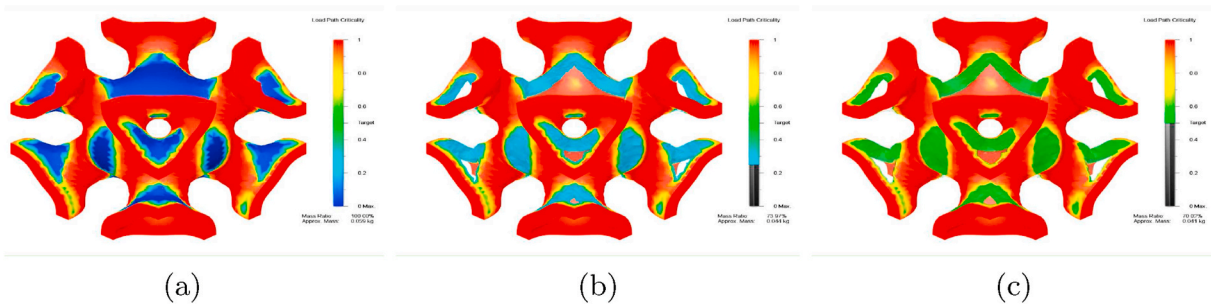


Fig. 10. I-WP lattice cell topology optimization under uniaxial compression loading: (a) 0% volume reduction, (b) 15% volume reduction, (c) 30% volume reduction.

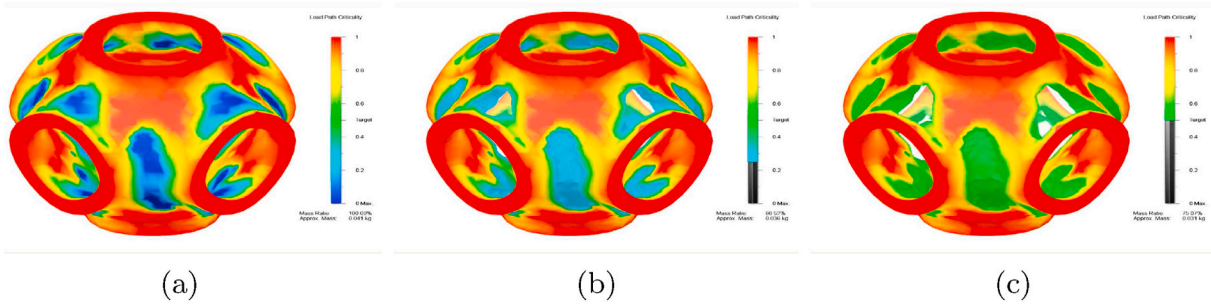


Fig. 11. Primitive lattice cell topology optimization under uniaxial compression loading: (a) 0% volume reduction, (b) 15% volume reduction, (c) 30% volume reduction.

element size and location. Once again, the largest average element size that produced a consistent result was used in further simulations.

The stress field for the optimized Diamond lattice design is presented in Fig. 12a. There was a noticeable change in the stress field from the base cell design to the optimized design. While there was a peak stress of

twice the peak stress value observed in the base condition, 1, 248.17 MPa, it was located along a sharp feature within the optimized mesh along the lower surface where an interior cell was removed during optimization, which caused an artificial stress concentration point at the feature. This stress concentration point was determined to be artificial

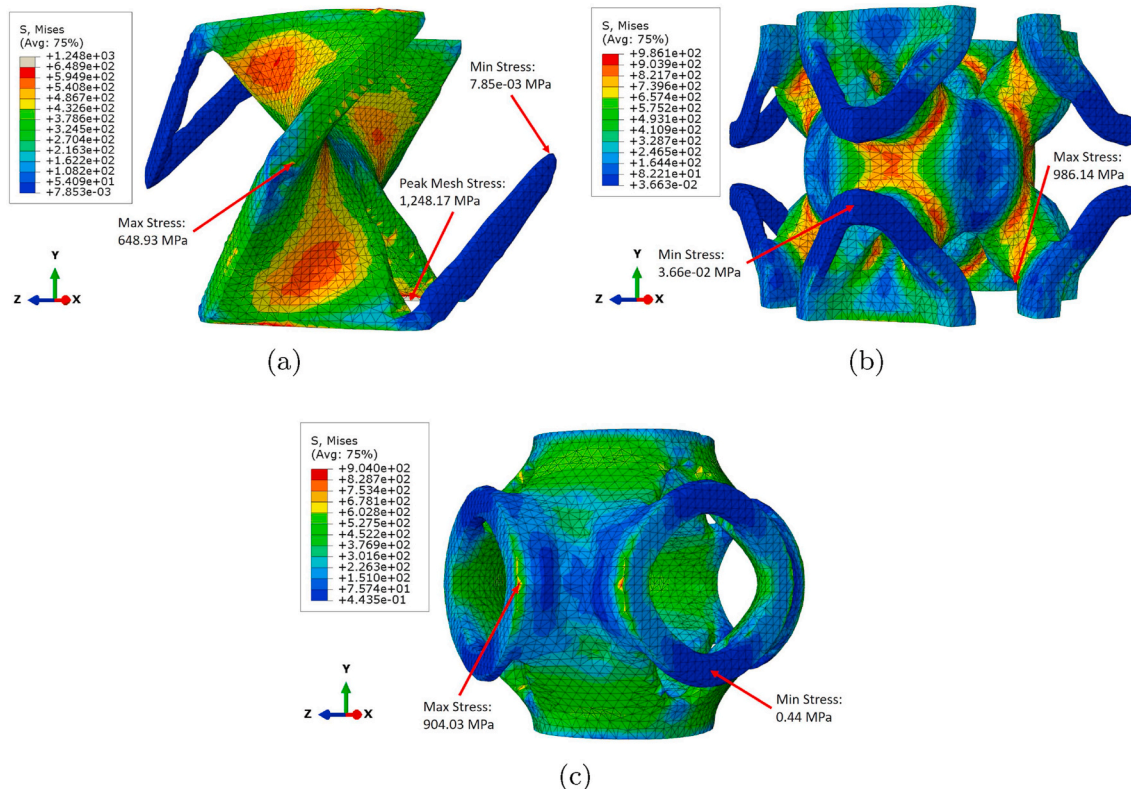


Fig. 12. Stress field under uniaxial compression for topology optimized unit lattice cell: (a) Diamond lattice, (b) I-WP lattice, (c) primitive lattice.

due to the location along a symmetry bounded face, as well as a comparison of the stress values found in the adjacent elements. Outside of this localized stress concentration, the maximum stress value observed was 648.93 MPa, located at the mid-surface hinge of the lattice cell. This could be another mesh artifact, when comparing the stress value in this location on the optimized cell to that of the base cell, although the hinge point along the surface edge would also lead to a stress concentration point. The stress value within the optimized cell stress field at the maximum stress location of the base cell was 611.79 MPa. This equates to a 1.11% decrease in the maximum stress value for a 30.94% decrease in cell volume and a 6.77% decrease in the stress value located along the mid-surface ridge, which is a meaningful gain in the cell's performance under uniaxial compression loading. The location of minimum stress for the Diamond lattice remained the same, with a 77% reduction in stress value.

The results for the optimized I-WP lattice design can be seen in Fig. 12b. The stress field pattern did not change significantly for the optimized I-WP lattice cell, although the stress values themselves saw a marked change. The peak stress for the I-WP cell was still located along one of the connecting arms of the lattice, as was the case for the base cell; however, in this case, the maximum stress value was only 986.14 MPa, a reduction of 62.63%. Optimization provided an even more significant gain for the I-WP lattice, with the 62.63% reduction paired with a 29.98% reduction in volume and mass. The minimum stress value within the lattice cell field was also reduced, this time by 99.64%. The minimum stress location of the base I-WP cell was removed during the optimization process, and within the optimized cell was located along the connecting face with an adjacent cell.

Finally, the stress field for the optimized Primitive cell can be found in Fig. 12c. As with the optimized I-WP lattice, the stress field of the optimized Primitive lattice cell remained relatively similar, even maintaining the exact locations for maximum and minimum stress values within the field. Unlike the previous two lattice cell designs, the optimized Primitive lattice cell saw an increase in maximum stress, up to a value of 904.03 MPa, which equates to a 7.81% increase. Considering the 24.93% decrease in cell volume, this can still be regarded as a net gain for the optimized Primitive cell's performance. The minimum stress value for the optimized cell was 0.44 MPa, which is a 97.70% reduction in the stress value.

Table 2 displays the changes in cell volume, maximum stress, and minimum stress values for each of the three lattice cases.

6. Conclusions

This study was focused on applying topology optimization methods, specifically the SIMP methodology, to an individual cell of a lattice design. As the method used within the FEA software for this research was not specific to the PMS lattice cells under investigation, these techniques could be applied to other lattices or cellular designs taking into account the loading conditions and constraints applied within the simulation. One constraint on the optimization process used here was that the cells retain the ability to be replicated into sheet lattices for use in engineering applications, there is some question as to how the optimized cells would perform when replicated. That is, if the change in topology would lead to a subsequent shift in overall mechanical properties. Furthermore, the loading condition used for optimization was under uniaxial compression within the initial loading response of the lattice cell. The optimized cell response beyond this condition will require further examination as well.

As a whole, this case study is an example of how topology optimization can prove successful, as the process was able to develop new cell designs intended to maximize lattice performance under the prescribed loading condition. Across all three optimized cell designs, the optimized cell saw an improved stress field response when considering the reduction in cell volume and subsequent reduction in mass. Even without considering the mass reduction, the Diamond and I-WP lattice

Table 2

Comparison of optimized and base condition cell for three lattice designs.

Optimized Cell Base Design	Volume Reduction (%)	Maximum Stress (MPa)	Maximum Stress Change from Base Cell (%)	Minimum Stress (MPa)	Minimum Stress Change from Base Cell (%)
Diamond	30.94	648.93	-1.11	0.20	-77.00
I-WP	29.98	986.14	-62.63	0.01	-99.64
Primitive	24.93	904.03	7.81	0.44	-97.70

cells showed improved performance. The I-WP lattice saw the most improvement through the topology optimization process, with a 62.63% decrease in maximum stress loading along with a 29.98% reduction in cell volume. Overall, topology optimization proved beneficial for designing TPMS-based lattice cells under an initial uniaxial loading condition.

Funding

This work is supported by the Air Force Office of Scientific Research Dynamic Materials and Interactions office of the Air Force Research Laboratory.

Credit author statement

Derek Spear: Conceptualization, Methodology, Investigation, Software, Formal Analysis, Data Curation, Writing – Original Draft, Writing – Review & Editing; Jeremiah Lane: Conceptualization, Methodology, Writing – Original Draft; Anthony Palazotto: Resources, Supervision, Project Administration; Ryan Kemnitz: Resources, Supervision, Funding Acquisition.

Data availability

The datasets generated and/or analyzed during the current study are available from the corresponding author on reasonable request.

Declaration of competing interest

The authors declare that they have no known competing financial interests or personal relationships that could have appeared to influence the work reported in this paper.

Acknowledgements

The authors would like to thank Dr. Martin Schmidt of the Air Force Office of Scientific Research for his support of this research.

References

- [1] Dassault Systèmes, Abaqus Unified Finite Element Analysis Software, 2016.
- [2] Autodesk, Fusion 360 Unified Computer Aided Design and Computer Aided Modeling Software, 2020.
- [3] C. Korner, Additive manufacturing of metallic components by selective electron beam melting — a review, *Int. Mater. Rev.* 61 (5) (2016) 361–377, <https://doi.org/10.1080/09506608.2016.1176289>.
- [4] O. Al-Ketan, R. Rowshan, R.K. Abu Al-Rub, Topology-mechanical property relationship of 3D printed strut, skeletal, and sheet based periodic metallic cellular materials, *Additive Manuf.* 19 (January) (2018) 167–183, <https://doi.org/10.1016/j.addma.2017.12.006>.
- [5] O. Al-Ketan, R. Rowshan, A.N. Palazotto, R.K. Abu Al-Rub, On mechanical properties of cellular steel solids with shell-like periodic architectures fabricated by selective laser sintering, *J. Eng. Mater. Technol. Trans. ASME* 141 (2) (2019) 1–12, <https://doi.org/10.1115/1.4041874>.
- [6] O. Al-Ketan, R.K. Abu Al-Rub, Multifunctional mechanical metamaterials based on triply periodic minimal surface lattices, *Adv. Eng. Mater.* 21 (10) (2019) 1–39, <https://doi.org/10.1002/adem.201900524>.

- [7] D. Spear, A.N. Palazotto, R. Kemnitz, Survivability and damage modeling of advanced materials, *Survivability: Papers Presented at the AIAA SciTech Forum and Exposition 2020* (2020) 123–134, <https://doi.org/10.2514/6.2020-1217>.
- [8] D. Spear, A.N. Palazotto, R. Kemnitz, First cell failure of lattice structure under combined loading, *AIAA Scitech 2021 Forum* (2021), <https://doi.org/10.2514/6.2021-0101>, 1–16.
- [9] D. G. Spear, A. N. Palazotto, Investigation and statistical modeling of the mechanical properties of additively manufactured lattices, *Materials* 14 (14). doi: 10.3390/ma14143962.
- [10] A. Asadpoure, L. Valdevit, Topology optimization of lightweight periodic lattices under simultaneous compressive and shear stiffness constraints, *Int. J. Solid Struct.* 60–61 (2015) 1–16, <https://doi.org/10.1016/j.ijsolstr.2015.01.016>.
- [11] D. Da, J. Yvonnet, L. Xia, M.V. Le, G. Li, Topology optimization of periodic lattice structures taking into account strain gradient, *Comput. Struct.* 210 (2018) 28–40, <https://doi.org/10.1016/j.compstruc.2018.09.003>.
- [12] Y. Du, H. Li, Z. Luo, Q. Tian, Topological design optimization of lattice structures to maximize shear stiffness, *Adv. Eng. Software* 112 (2017) 211–221, <https://doi.org/10.1016/j.advengsoft.2017.04.011>.
- [13] P. Liu, Z. Kang, Y. Luo, Two-scale concurrent topology optimization of lattice structures with connectable microstructures, *Additive Manuf.* 36 (2020) 101427, <https://doi.org/10.1016/j.addma.2020.101427>.
- [14] B. Hanks, M. Frecker, 3d additive lattice topology optimization: a unit cell design approach, *Proceedings of the ASME Design Engineering Technical Conference, 46th Design Automation Conference (DAC)*doi:10.1115/DETC2020-22386.
- [15] D.G. Spear, A.N. Palazotto, R.A. Kemnitz, Mechanical properties of additively manufactured periodic cellular structures and design variations, *J. Eng. Mater. Technol.* (2021) 1–48, arXiv:<https://asmedigitalcollection.asme.org/materialstechnology/article-pdf/doi/10.1115/1.4050939/6685768/mats-21-1037.pdf>, doi:10.1115/1.4050939. URL <https://doi.org/10.1115/1.4050939>.
- [16] L. Xia, Topology optimization framework for multiscale nonlinear structures, in: L. Xia (Ed.), *Multiscale Structural Topology Optimization*, Elsevier, 2016, pp. 1–19, <https://doi.org/10.1016/B978-1-78548-100-0.50001-X>.
- [17] J. Gao, H. Li, Z. Luo, L. Gao, P. Li, Topology optimization of micro-structured materials featured with the specific mechanical properties, *Int. J. Comput. Methods* 17 (2018) 1850144, <https://doi.org/10.1142/S021987621850144X>.
- [18] L. Xia, P. Breitkopf, *Multiscale Structural Topology Optimization, 11th World Congress on Structural and Multidisciplinary Optimization, 2015*, pp. 1–6.
- [19] M. Zhou, Y.K. Shyy, H.L. Thomas, Checkerboard and minimum member size control in topology optimization, *Struct. Multidiscip. Optim.* 21 (2) (2001) 152–158, <https://doi.org/10.1007/s001580050179>.
- [20] X. Huang, Y.M. Xie, M.C. Burry, Advantages of bi-directional evolutionary structural optimization (beso) over evolutionary structural optimization (eso), *Adv. Struct. Eng.* 10 (6) (2007) 727–737, <https://doi.org/10.1260/136943307783571436>.
- [21] H. Eschenauer, N. Olhoff, Topology optimization of continuum structures: a review, *Appl. Mech. Rev.* 54 (2001) 331–390, <https://doi.org/10.1115/1.1388075>.
- [22] O. Sigmund, K. Maute, Topology optimization approaches: a comparative review, *Struct. Multidiscip. Optim.* 48 (6) (2013) 1031–1055, <https://doi.org/10.1007/s00158-013-0978-6>.
- [23] L. Li, K. Khandelwal, Topology optimization of structures with length-scale effects using elasticity with microstructure theory, *Comput. Struct.* 157 (2015) 165–177, <https://doi.org/10.1016/j.compstruc.2015.05.026>.
- [24] M. Jiang, I. Jasiuk, M. Ostoja-Starzewski, Apparent elastic and elastoplastic behavior of periodic composites, *Int. J. Solid Struct.* 39 (1) (2002) 199–212, [https://doi.org/10.1016/S0020-7683\(01\)00145-7](https://doi.org/10.1016/S0020-7683(01)00145-7).
- [25] S. Li, Boundary conditions for unit cells from periodic microstructures and their implications, *Compos. Sci. Technol.* 68 (9) (2008) 1962–1974, <https://doi.org/10.1016/j.compscitech.2007.03.035>.